FLUIDELASTIC FORCES IN A TRIANGULAR TUBE BUNDLE SUBJECTED TO TWO-PHASE CROSS FLOW

Njuki Mureithi, Soroush Shahriary, Emmanuelle Sommier, Michel Pettigrew,
École Polytechnique

1. INTRODUCTION

There are two general approaches for modeling fluidelastic instability: (i) truly analytical models requiring little or no experimental fluid force data; (ii) analyses requiring experimental fluid force data which may be either the fully unsteady data or steady time averaged data (Price & Païdoussis 1986). The first category, because of the complexity of the physics, cannot be adapted and the analyses using unsteady data requires a vast amount of experimental work while the quasi-static theory can provide a fairly acceptable solution with a reasonable number of experiments.

The quasi-static theory is widely used in the study of aeroelasticity and flow induced vibrations. This theory uses static fluid force coefficients measured on a stationary body to estimate motion induced fluid forces on an oscillating body, supposing that at any instant in time the body is moving with a constant velocity equal to the actual instantaneous value of the real velocity. It is known that this assumption is only valid for high values of the reduced velocity (Granger & Païdoussis 1996).

For a tube in a tube bundle the reduced velocity is not very high (in our case it is of the order of one). So the pure quasi-static assumption cannot lead to a realistic solution and it is not even possible to predict the fluidelastic instability for a single flexible cylinder for two-phase flow and air flow (Price & Païdoussis 1983) although the fluid force coefficient variations show that it is possible to predict fluidelastic instability in water flow (with pure quasi-static assumption).

The quasi-static model can be improved if the effect of flow retardation (Simpson and Flower 1977) or the effect of fluid inertia as interpreted by Lever and Weaver (1982) is taken into account. Using the quasi-static theory along with time delay enables one to predict instability both in lift and drag directions. The simplicity of using this approach along with it's capability to give qualitative agreement with experiments makes it a good candidate for the prediction of fluidelastic instability. It is also possible to go further and use the more elaborated quasi-unsteady method (Granger & Païdoussis 1996).

The main objectives of this study are: (i) explicit determination of the fluid force coefficients based on measured data in two-phase (air-water) flow; (ii) investigation of the physics of fluidelastic instability using the force coefficients in single phase and two-phase flow;(iii) to provide a comprehensive data base for future work on the prediction of fluidelastic instability using quasi-steady or quasi-unsteady approaches; (iv) provide fluidelastic instability information for modeling and tube wear prediction.

2. THEORETICAL BACKGROUND

The early eighties saw a proliferation of theoretical models for the prediction of fluidelastic instability. These models, developed for single phase flows, are primarily identified by their degree of complexity and level of empiricism. The group of "wavy-wall" models developed by Weaver and co-workers (1982, 1993) at McMaster University are probably the most analytical, requiring minimal empirical input. At the other extreme is the general unsteady model developed by Chen (1983) at Argonne National Laboratory. Chen's model is probably the most accurate, but also the most 'labor intensive' requiring a large number of coefficients to be measured in complex dynamic tests. The model has, however, been credited with clarifying the basic mechanisms underlying fluidelastic instability.

The group of quasi-static/quasi-steady models developed by Price and Païdoussis (1983, 1984, and 1986) at McGill University presents a compromise by introducing a simplified analytical model for the velocity effects. For this reason only displacement dependent forces need to be determined experimentally; significantly reducing the effort required to obtain empirical inputs.
The work reported here is part of a research program aimed at investigating the feasibility of adapting existing single phase flow models to the more complex two-phase flow problem. The quasi-steady approach has been selected in view of its moderate complexity while still remaining reasonably realistic. To highlight the role played by the fluid forces to be presented here, the basic quasi-static model for the group of cylinders subjected to cross-flow in Figure 1 is briefly demonstrated.

This group of cylinders may be part of a much larger array. For simplicity, assume that the array is constrained such that only cylinders '1' and '2' are free to vibrate, and only in the directions x_1 and y_2, respectively; thus a two-degree-of-freedom system. The governing equations of motion, when the tubes are modeled as 1 d.o.f. oscillators, are

$$\begin{aligned} m\ddot{x}_1 + c\dot{x}_1 + kx_1 &= f_1(x_1, \dot{x}_1, \ddot{x}_1, y_2, \dot{y}_2, \ddot{y}_2, U) \\ m\ddot{y}_2 + c\dot{y}_2 + ky_2 &= g_2(x_1, \dot{x}_1, \ddot{x}_1, y_2, \dot{y}_2, \ddot{y}_2, U). \end{aligned} \tag{1}$$

The quasi-static assumption postulates that the fluid forces (f_1, g_2) may be simplified to first order functions of positions only, thus

$$f_1(.) = \frac{1}{2}\rho U^2 lD\left(C_{D10} + \frac{\partial C_{D1}}{\partial x_1} x_1 + \frac{\partial C_{D1}}{\partial y_2} y_2 \right) \tag{2}$$

and

$$g_2(.) = \frac{1}{2}\rho U^2 lD\left(C_{L20} + \frac{\partial C_{L2}}{\partial x_1} x_1 + \frac{\partial C_{L2}}{\partial y_2} y_2 \right). \tag{3}$$

The quasi-static assumption thus 'ignores' the velocity dependence in the fluid forces. To correct for this, as well as account for the variable angle of attack during vibration, the more general quasi-steady (Price & Païdoussis, 1983) and quasi-unsteady (Granger & Païdoussis, 1996) models have been developed. For purposes of the present demonstration, equations (2) and (3) will be retained. Introducing these equations into the equations of motion (1) yields

$$[M]\ddot{\vec{X}} + [C]\dot{\vec{X}} + [K]\vec{X} = \vec{F}_0 \tag{4}$$

where

$$[M] = \begin{bmatrix} m & 0 \\ 0 & m \end{bmatrix},\ [C] = \begin{bmatrix} c & 0 \\ 0 & c \end{bmatrix},\ [K] = \begin{bmatrix} \bar{k}_{11} & \bar{k}_{12} \\ \bar{k}_{21} & \bar{k}_{22} \end{bmatrix}, \tag{5}$$

and

$$\begin{aligned} \bar{k}_{11} &= k - \frac{1}{2}\rho U^2 lD \frac{\partial C_{D1}}{\partial x_1} x_1,\ \ \bar{k}_{12} = -\frac{1}{2}\rho U^2 lD \frac{\partial C_{D1}}{\partial y_2} y_2, \\ \bar{k}_{21} &= -\frac{1}{2}\rho U^2 lD \frac{\partial C_{L2}}{\partial x_1} x_1, \quad \bar{k}_{22} = k - \frac{1}{2}\rho U^2 lD \frac{\partial C_{L2}}{\partial y_2} y_2. \end{aligned} \tag{6}$$

A stability analysis of equation (4) (Païdoussis and Price, 1988) shows that the critical fluidelastic instability velocity, U_c, for the simplified model of Figure 1 is given by

$$\frac{U_c}{fD} = K\left(\frac{m\delta}{\rho D^2}\right)^{1/2} ; \quad K = \left[\frac{-256\pi^2}{(\bar{k}_{11} - \bar{k}_{22}) + 4\bar{k}_{12}\bar{k}_{21}}\right]^{1/4}. \tag{7}$$

Equation (7) reveals the well known Connors equation relating the critical velocity to the mass-damping parameter. More importantly, it is demonstrated that the Connors constant K depends closely on the fluid force (stability) derivatives of equation (6). The Connors constant is extremely important since current nuclear steam generator design guidelines depend on knowledge of this 'constant'.

The Connors constant has also been employed in non-linear dynamics computer codes used to estimate tube wear during fluidelastic instability. The constant is employed in a form of 'reverse engineering' to estimate the energy generated by the fluidelastic instability mechanism. In essence, the exercise replaces the fluid forces derivatives in equation (7) by the single constant K. It is clear that this is an oversimplification of the physics of the problem – raising doubts about the validity of the estimated energy. A valid estimate of the energy generation mechanism requires direct numerical simulation of equation (4). It is therefore evident that the fluid forces are needed for such an analysis.

The foregoing brief exposé is the background surrounding the work reported here. The primary goal of the work is therefore to determine the fluid force derivatives that could be employed in a stability analysis as done in equations (4-7), and also in a non-linear analysis for the estimation tube wear rates under instability conditions.

3. EXPERIMENTAL METHOD

3.1 Test Apparatus

The air-water two-phase flow loop of the Fluid-Structure Interactions Laboratory at École Polytechnique de Montreal was used for the experimental measurements. The loop comprises a 25 l/s variable speed pump, a magnetic flow meter, a 2500 l tank, a 250 l/s and compressed air supply system and connecting piping as shown in Figure 2.

The compressed air was injected below a suitably designed mixer to homogenize and distribute the two-phase mixture uniformly below the test-section. The air flow was measured with orifice plates connected to a differential pressure transducer and electronic readout system. The loop was operated at room temperature and the pressure in the test- section was slightly above atmospheric. The test-section, which has an essentially rectangular cross section (99 x 191 mm), is shown in Figure 3. It consists of three columns of 38 mm diameter cylinders flanked on either side by half cylinder columns to simulate essentially the flow path in a large array of cylinders in a rotated triangular configuration. The pitch-to-diameter ratio, P/D, was 1.5, corresponding to an inter-cylinder gap of 19 mm. To measure the quasi-static fluid forces, the following key components were designed and fabricated:

(i) Force balance (dynamometer), the force measurement system for the primary measurement tube;
(ii) X-Y traverse mechanism for displacement and positioning of the primary measurement tube;
(iii) Strain-gauge instrumented cylinders for the measurement of cross-coupling forces between the primary cylinder and its neighbors.

A schematic view of the miniature dynamometer, measuring 60 mm in height, is presented in Figure 4. The instrument consists of two pairs of thin beams mounted such that $x-y$ cross-coupling is essentially eliminated. Sealing the strain gauges on the beams proved to be a challenge. A photo of the actual system is shown in Figure 4(b).

The primary test cylinder is mounted on the dynamometer enabling the measurement of fluid forces transverse to the cylinder axis. Figure 5 shows the dynamometer calibration curves. Figure 5(a) shows that the two pairs of beams have nearly identical calibrations. Note also that cross coupling between the x- and y-directions is negligible. This is crucially important for the present tests due to the generally large difference between the lift and drag forces. Figure 5(b) shows the force deformation relationship when the calibration weight is placed either at the center (M) of the cylinder or the extremity (E) away from the force balance. In both case identical readings are obtained; thus force variations along the cylinder axis do not affect the force balance output.

Figure 6 shows the traverse mechanism on which the dynamometer is mounted. Electronic potentiometers measure the primary cylinder position within the tube bundle to within 0.3 mm.

3.2 Test Procedure

The group of 7 cylinders under investigation is shown in Figure 7. In this paper, the force measurements for only the cylinders labeled C, 1, 2, 3 & 4 are reported. The central cylinder 'C', which is mounted on the force balance, was displaced in the drag ($x-$) and lift ($y-$) directions in increments of 0.028D within the area marked 'test area' in the figure. At each position, the flow was allowed to settle and then data acquisition was performed over a duration of one minute. The average lift and drag forces were then computed for each cylinder.

Test results are presented in the form of force coefficients C_D and C_L as functions of the dimensionless displacements $\tilde{x}$ or $\tilde{y}$ of cylinder 'C'. The force coefficients, for a given cylinder, are calculated based on the pitch velocity U_p as

$$C_D = \frac{F_D}{\frac{1}{2}\rho U_p^2 lD}$$
$$C_L = \frac{F_L}{\frac{1}{2}\rho U_p^2 lD} \quad (8)$$

Where F_D and F_L are the measured drag and lift forces, respectively. Table 1 shows the flow parameters varied during the tests. The void fraction β in table 1 is the superficial void fraction and U_p stands for homogeneous pitch flow velocity.

Void fraction β (%)	Flow velocity (U_p m/s)
0	1.84
60	4.93
80	4.96

Table 1 Test Conditions

5. RESULTS AND DISCUSSION

5.1 Fluid force coefficients in two-phase flows

In all the results that follow, the measured force coefficients are presented as functions of the central cylinder, 'C', dimensionless displacements $\tilde{x}$ and $\tilde{y}$. For cylinders 1-4, the force coefficients directly represent the coupling effect associated with motion of the central cylinder on its neighbors (Figure 7).

The primary set of results to be presented is that for 80% homogeneous void fraction. This is the void fraction of interest within the U-bend region of nuclear steam generators. Figure 8 shows the measured lift and drag coefficients for cylinder 'C'. The lift coefficient remains essentially zero when the cylinder is displaced in the drag direction, Figure 8(a). This makes sense from symmetry considerations. The drag coefficient increases as the cylinder is displaced in the downstream direction, Figure 8(b). The slight increase may be associated with increased blockage of the flow channels downstream of the cylinder.

The lift coefficient is strongly dependent on the transverse displacement ($\tilde{y}$). As seen in Figure 8(b), the lift force is always directed toward the cylinder equilibrium (zero) position. The same behavior was found by Païdoussis et al., (1996) in air flow tests. The negative value of the derivative $\partial C_{LC}/\partial\tilde{y}$ was shown to directly determine instability in the quasi-steady model. For cylinder 'C', C_{DC} only varies slightly with transverse displacement $\tilde{y}$. In particular the derivative $\partial C_{DC}/\partial\tilde{y}\big|_{\tilde{y}=0} = 0$; as would be expected from symmetry considerations. The effect of tube 'C' displacement on tube 1 lift (C_{L1}) and drag (C_{D1}) forces is shown in Figure 9. Tube 1 is located directly downstream of tube 'C'. Inline ($\tilde{x}$) displacement of tube 'C' leaves C_{LC}

unaffected; C_{DC} shows a decreasing trend as the cylinder falls in the wake of cylinder 'C'. Transverse displacement ($\tilde{y}$) has a strong effect on the cylinder 1 lift coefficient, C_{L1}, Figure 9(b).

The displacement of cylinder 'C' has the strongest effect on tube 'C' itself, and tube 1 immediately downstream where C_L varies significantly with ($\tilde{y}$) in both cases. As seen in figures 10 and 11 cylinders 2 and 3 in the neighbouring column show less sensitivity to tube 'C' displacements. The lift coefficients of cylinders 2 and 3 are essentially unchanged in Figures 10(a) and 11(a) for the displacement of tube 'C' in x-direction. The tube 2 and 3 drag coefficients show an increasing trend with ($\tilde{x}$) for both cylinders. Interestingly, C_{D2} increases as cylinder 'C' approaches cylinder 2 in the traverse direction, while C_{D3} is insensitive to $\tilde{y}$ displacements.

Figure 12 shows the results for tube 4, located directly upstream of tube 'C'. The displacements of tube 'C' only has a measurable effect on the drag coefficient C_{D4} when cylinder 'C' is displaced parallel to the flow direction, Figure 12(c).

Tests at 60% superficial void fraction yielded force coefficient variations remarkably close to those measured for 80% void fraction above. Figure 13 shows a comparison of the force coefficients for cylinder 'C' at these two superficial void fractions. The lift coefficient (C_{LC}) variation is practically identical at the two void fractions. The equality of the derivatives $\partial C_{LC}/\partial\tilde{y}$ indicates that the displacement $\tilde{y}$ has the same effect on stability in both cases. The drag coefficient values are slightly lower at 60% void fraction.

A comparison of tube 1 force coefficients for the two void fractions is shown in figure 14. In this case the force coefficients are even closer. Although not shown here, the force coefficients for cylinders 2-4 show similar characteristics. The drag coefficient remains higher at 80% void fraction.

5.2 Comparison with single phase flow

Fluid forces have also been measured in water flow ($\beta = 0\%$). The results for the primary cylinder 'C' are presented in Figure 15. The most distinct difference is in the variation of C_{LC} with the traverse displacement $\tilde{y}$. While the steady lift force is directed towards the cylinder equilibrium position in the high void fraction two-phase flow case, it is directed in the opposite direction for water flow, Figure 15(b). The lift coefficient variation previously presented in air flow by Païdoussis *et al.*, (1996) is also shown. The derivative $\partial C_{LC}/\partial\tilde{y}$ varies continuously from a positive value at 0% void fraction to a large negative value at 100% void fraction. For the drag coefficient variation in Figure 15(d), it should be noted that C_{DC} has a local maximum at $\tilde{y}$=0 for water flow, but a minimum at 60% and 80% void fractions.

5.3 Force coefficient derivatives

In the stability analysis outlined in Section 2, it was demonstrated that for the quasi-steady theory, the derivatives $\partial C_{Li}/\partial\tilde{x}$, $\partial C_{Di}/\partial\tilde{x}$ etc. are the necessary inputs to the model, see equations (4)-(7). These derivatives, at ($\tilde{x} = 0$, $\tilde{y}$=0) are estimated from the data of figures 8-15, as well as other results not presented here for brevity.

Table 2 shows the force coefficients C_D, C_L as well as the derivatives with respect to tube 'C' displacements. To determine the derivatives, a third order polynomial fit of the test data was performed. The derivative sought then corresponded to the coefficient of the linear term.

For both void fraction values, $\beta = 60\%$, $\beta = 80\%$, the derivative $\partial C_{LC}/\partial\tilde{y}$ is the most important; indicating that tube 'C' transverse displacement has the most influence on the tube 'C' fluid forces. The next largest influence is that on tube 1 immediately downstream again in the lift direction. This is followed by tube 2 affected in the drag direction. Figure 16 shows a visual

representation of the influence of tube 'C' on its neighbors for lift or drag direction displacements. The length and thickness of the arrows reflect the level of influence. Only the most significant effects are shown.

The results for $\beta = 80\%$ and $\beta = 60\%$ are closely similar, except for the significantly larger derivatives for $\partial C_{D4} / \partial \tilde{x}$ for $\beta = 80\%$ superficial void fraction. Besides the effect the force field on itself, tube 'C's influence is felt by the tubes downstream. Tubes in the same column are also significantly affected even when located downstream of the moving tube. However it should be noted that the upstream tube 4 is affected in the drag direction, while the downstream tube 1 is influenced in lift direction.

Figure 16 and Table 2 give useful insights into the stability behavior of the tube bundle. Test results reported by Violette *et al.*(2006) show that the orbital motion for a group of seven cylinders within a rigid bundle is as shown in Figure 17, for $\beta = 80\%$ .The tubes are axisymmetrically flexible. Cross-flow amplitudes are dominant, supporting the importance of the derivative $\partial C_{LC} / \partial \tilde{y}$. In another test with a column of flexible tubes, it was found that instability occurred when tubes were flexible in the lift direction, but no instability occurred when tubes were flexible only in the drag direction. This may be expected from the weaker coupling in the drag direction as reflected by the derivatives $\partial C_D / \partial \tilde{x}$. When an adjacent flexible column was added, instability did occur in the flow direction highlighting the importance of the role played by derivatives such as $\partial C_{D2} / \partial \tilde{x}$.

The natural continuation of this work involves quantitative stability analysis of the tube bundle employing the force derivatives of table 2. This is currently under way.

6. Conclusions

Lift and drag coefficients have been measured for a rotated-triangle tube bundle subjected to two-phase flow. A centrally located tube was displaced in the cross-flow and inflow directions and forces coefficients measured on the tube itself as well as on four of the closest neighbors. The inter-tube couplings, represented by the derivatives $\partial C_L / \partial \tilde{y}$, $\partial C_L / \partial \tilde{x}$ etc., were of primary interest.

In comparison to single phase flow, inter-tube coupling was found to be weaker in two-phase flow. Tube displacement were found to mainly affect the group of tubes downstream of the displaced tube in the case of two-phase flow while for single phase flow, it was the group of upstream tubes that was most affected. Tubes in the same column were found to be strongly coupled in the cross-flow direction but generally less so in the inflow direction.

The present results give added insight into recent stability tests in two-phase flow. For instance, the weak inflow coupling may explain why a single column of flexible tubes (within an otherwise rigid array) is unstable when free to vibrate in the cross-flow direction, but completely stable when only flexible in the inflow direction.

Possibly the most important contribution of the present work is the data base of fluid force derivatives themselves. The derivatives are the inputs needed for a quantitative stability analysis of a tube bundle subjected to two-phase flow. Furthermore, the nonlinear forces may be employed in direct numerical simulations of post instability behaviour of tube bundles which is necessary for tube wear estimation.

7. Acknowledgments

The authors are grateful to Christine Monnette who designed the two-phase flow test section. Thanks to Thierry Lafrance and Benedict Bésner for their assistance with aspects of data acquisition and instrumentation. Nour Aimène's expertise with strain gauges made it possible to have a high precision measurement system.

8. Nomenclature

c : Total damping (N.s/m)
C_D , C_L : Drag and lift coefficient
F_D , F_L : Force in drag and lift directions(N)
f : Frequency (Hz)
k : Stiffness (N /m)
m : Total mass (kg/m)
P , D , l : Pitch , tube diameter and tube length(m)
U : Mixture velocity
U_∞ , U_p , U_c : Free stream, pitch, critical pitch velocity (m/s)
x , y : Tube position in drag and lift direction (m)
$\tilde{x}$, $\tilde{y}$: Non dimensional displacements in drag and lift direction(x/D , y/D)
$\vec{X}, \dot{\vec{X}}, \ddot{\vec{X}}$: Displacement, velocity and acceleration vector (m, m/s and m/s^2)

β : Superficial void fraction
δ : Logarithmic decrement
ρ : Two-phase mixture density (kg/m^3)

9. REFERENCES

Chen, S.S., 1977,"A mathematical model for cross-flow induced vibrations of tube rows", 3rd International conference pressure vessel technology: 415-426.

Granger, S. and M. P. Païdoussis, 1996, "Improvement to the quasi-steady model with application to cross-flow-induced vibration of tube arrays", Journal of Fluid Mechanics **320**: 163-184.

Lever, J. H. and D. S. Weaver, 1982, "Theoretical model for fluid-elastic instability in heat exchanger tube bundles", Journal of Pressure Vessel Technology Transactions of the ASME **104**(3): 147-158.

Lever, J. H. and Rzentkowski G., 1993, "Dependence of post-stable fluidelastic behavior on the degrees of freedom of a tube bundle", Journal of fluids and structures **7**: 471-496.

Mureithi, N.W., Nakamura, T., Hirota, K., Murata, M., Utsumi, S., Kusakabe, T. and Takamatsu, H. ,2002, “Dynamics of an in-line tube array subjected to steam–water cross-flow part ii: unsteady fluid forces”, Journal of Fluids and Structures**16**: 137-152.

Païdoussis, M.P. , Price, S.J., 1988, “The mechanisms underlying flow-induced instabilities of cylinder arrays in cross-flow”, Journal of Fluid Mechanics **,187**,45-59.

Price, S. J. and M. P. Païdoussis, 1983, "Fluidelastic instability of an infinite double row of circular cylinders subject to a uniform cross-flow”, Journal of Vibration, Acoustics, Stress, and Reliability in Design **105**(1): 59-66.

Price, S. J. and M. P. Païdoussis , 1984 , “Theoretical investigation of the fluidelastic instability of a single flexible cylinder surrounded by rigid cylinders”, 1984, p 117-133.

Price, S. J. and M. P. Païdoussis, 1986, "A constrained-mode analysis of the fluidelastic instability of a double row of flexible circular cylinders subject to cross-flow: a theoretical investigation of system parameters", Journal of Sound and Vibration **105**, (1), 1986, p 121-142.

Price, S. J., M. P. Païdoussis and Giannias N., 1988, "A generalized constrained-mode analysis for cylinder arrays in cross-flow", International symposium on flow-induced vibration and noise **3**, 1988, p25-56.

Simpson, A. and J. W. Flower, 1977, "Improved mathematical model for the aerodynamic forces on tandem cylinders in motion with aero elastic applications", Journal of Sound and Vibration **51**(2): 183-217.

Violette R., Pettigrew, M.J., Mureithi N.W., 2006, “Fluidelastic instability of an array of tubes preferentially Flexible in the flow direction subjected to two-phase cross flow”, Transactions of the ASME **128**,148-159.

		C_D	C_L	$C_{D,\tilde{x}}$	$C_{L,\tilde{x}}$	$C_{D,\tilde{y}}$	$C_{L,\tilde{y}}$
Vp(m/s)= 3.93 $\beta = 60\%$	CENTRAL	0.44	0.01	0.11	0.01	0.02	-0.60
	TUBE1	0.48	-0.01	-0.10	0.00	-0.01	0.36
	TUBE2	0.43	-0.02	0.17	-0.05	-0.19	0.04
	TUBE3	0.54	0.00	0.09	0.00	0.04	0.06
	TUBE4	0.48	0.01	-0.07	0.11	0.15	0.02
		C_D	C_L	$C_{D,\tilde{x}}$	$C_{L,\tilde{x}}$	$C_{D,\tilde{y}}$	$C_{L,\tilde{y}}$
Vp(m/s)= 3.97 $\beta = 80\%$	CENTRAL	0.48	0.00	0.10	-0.01	-0.03	-0.58
	TUBE1	0.49	0.00	-0.13	0.04	0.02	0.32
	TUBE2	0.45	-0.03	0.15	-0.04	-0.21	0.05
	TUBE3	0.56	0.01	0.08	0.02	-0.04	-0.12
	TUBE4	0.51	-0.03	-0.25	0.06	0.13	0.04
		C_D	C_L	$C_{D,\tilde{x}}$	$C_{L,\tilde{x}}$	$C_{D,\tilde{y}}$	$C_{L,\tilde{y}}$
Vp(m/s)= 1.84 $\beta = 0\%$	CENTRAL	0.37	0.00	0.29	0.02	0.04	0.65
	TUBE1	0.42	0.02	0.01	-0.02	-0.02	-0.14
	TUBE2	0.40	0.00	0.07	0.06	0.12	-0.08
	TUBE3	0.40	-0.01	-0.22	0.14	-0.08	0.00
	TUBE4	0.41	0.00	0.16	0.01	-0.02	0.29
Data extracted from Price, S. J., *et al.* (1988)							
		C_D	C_L	$C_{D,\tilde{x}}$	$C_{L,\tilde{x}}$	$C_{D,\tilde{y}}$	$C_{L,\tilde{y}}$
Re=1.85x10^4 P/D=1.375 $\beta = 100\%$	CENTRAL	0.51	0	-0.39	0	0	-18.07
	TUBE1	-	-	-0.27	0	0	-0.98
	TUBE2	-	-	0.38	1.87	0.25	-1.98
	TUBE3	-	-	-2.63	0	-0.12	1.24
	TUBE4	-	-	0.28	0	0	-5.36

Table 2 Force coefficients and their derivatives

		C_D	C_L	$C_{D,\tilde{x}}$	$C_{L,\tilde{x}}$	$C_{D,\tilde{y}}$	$C_{L,\tilde{y}}$
Vp(m/s)= 1.84 $\beta = 0\%$ (no mixture)	CENTRAL	0.58	0.00	0.34	0.07	0.01	0.27

Table 3 Force coefficients and their derivatives (without mixture)

10. FIGURES

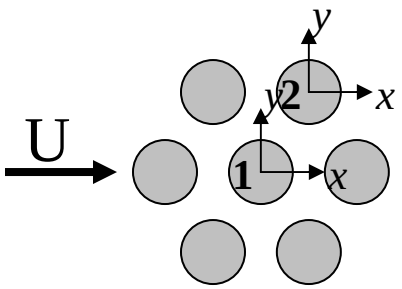

Fig. 1: Two flexible tubes in a tube bundle

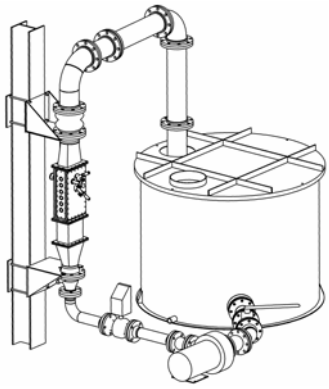

Fig. 2: Test loop

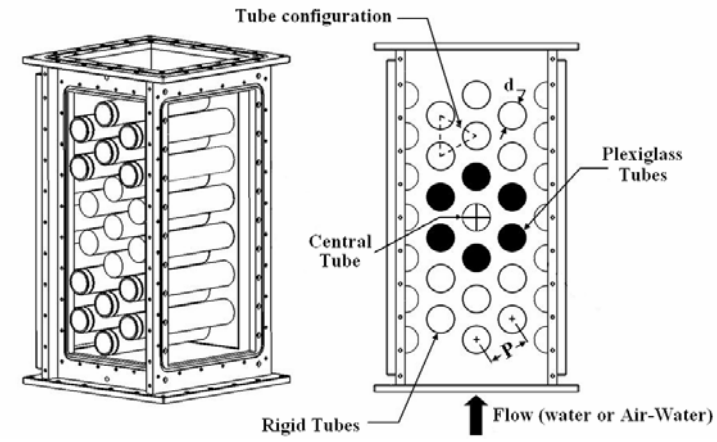

Fig. 3: Test section

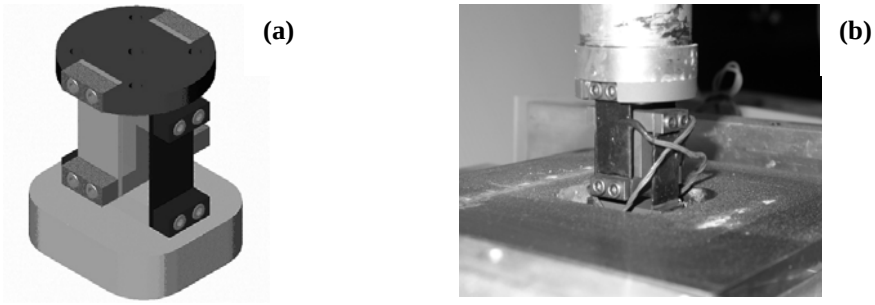

Fig. 4(a): Test section schematic view of dynamometer and, (b) photo of dynamometer mounted on force balance.

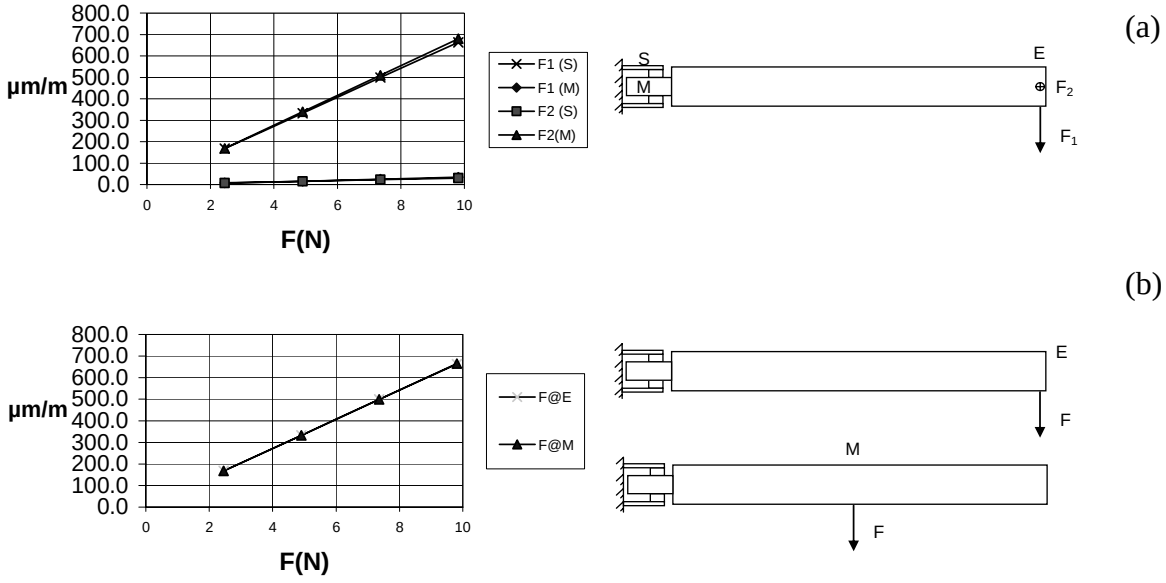

Fig. 5(a): Calibrations for the two dynamometer axes, (b) Calibrations comparison for two force locations 'E' and 'M'.

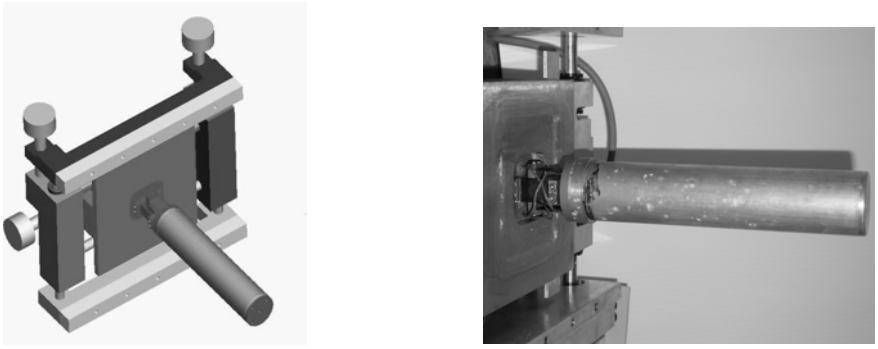

Fig. 6: x-y traverse system

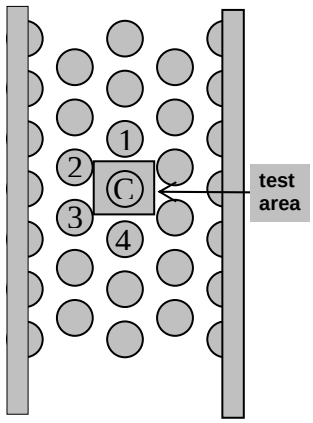

Fig. 7 Tube array showing test area of interest and instrumented cylinders.

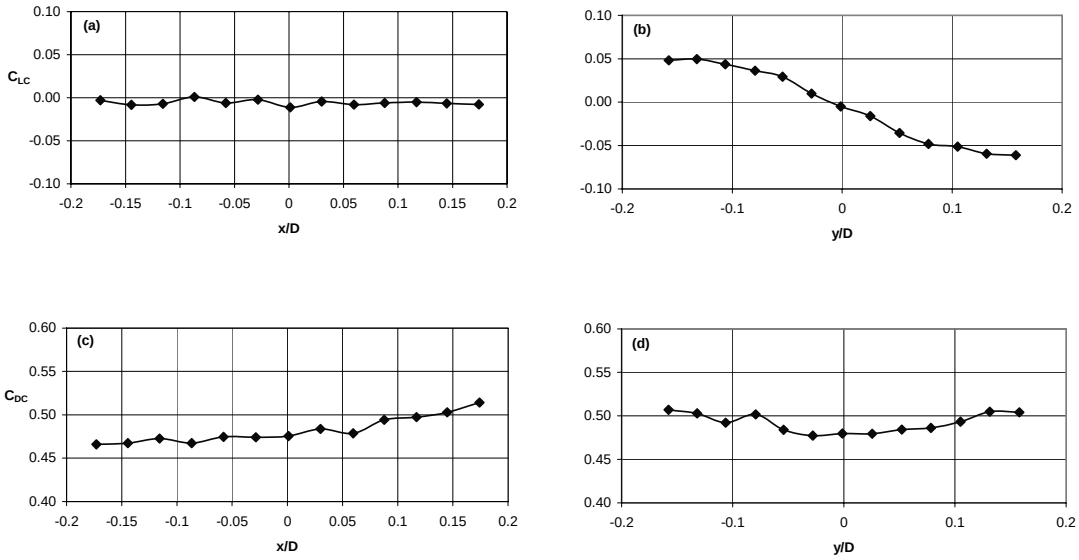

Fig. 8: Measured (a,b) lift and (c,d) drag force coefficients for the central cylinder, 'C', ($U_P = 3.96 m/s$, $\beta = 80\%$).

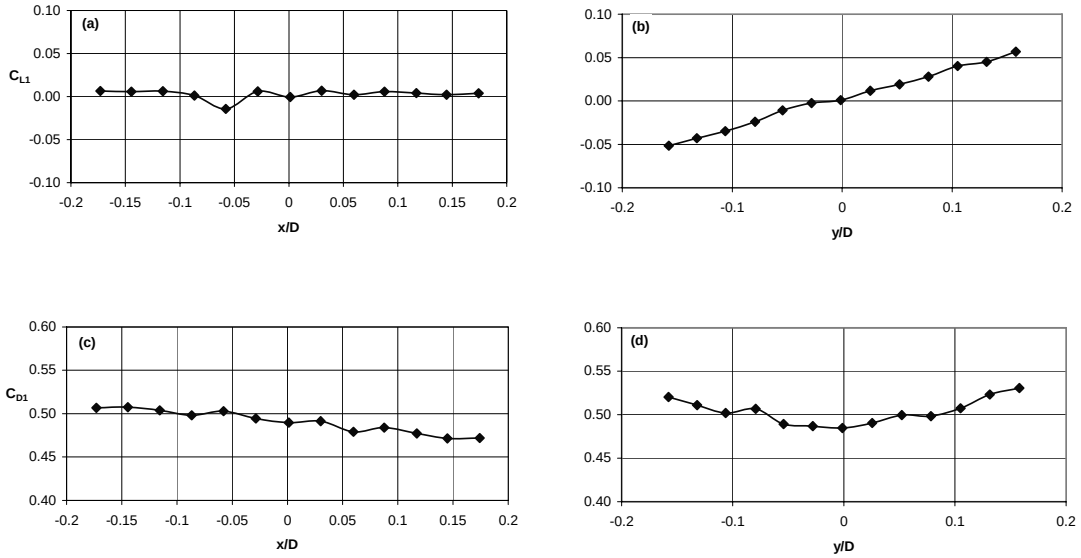

Fig. 9: The effect of tube 'C' displacement on the measured (a,b) lift and (c,d) drag force coefficients for tube 1 ($U_P = 3.96 m/s$, $\beta = 80\%$).

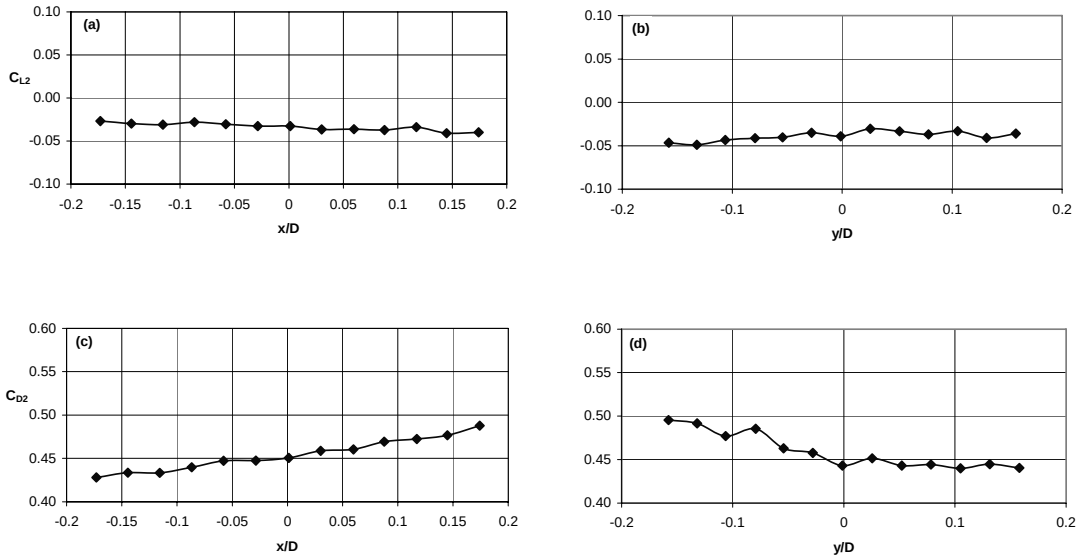

Fig. 10: The effect of tube 'C' displacement on the measured (a,b) lift and (c,d) drag force coefficients forces for tube 2 ($U_P = 3.96 m/s$, $\beta = 80\%$).

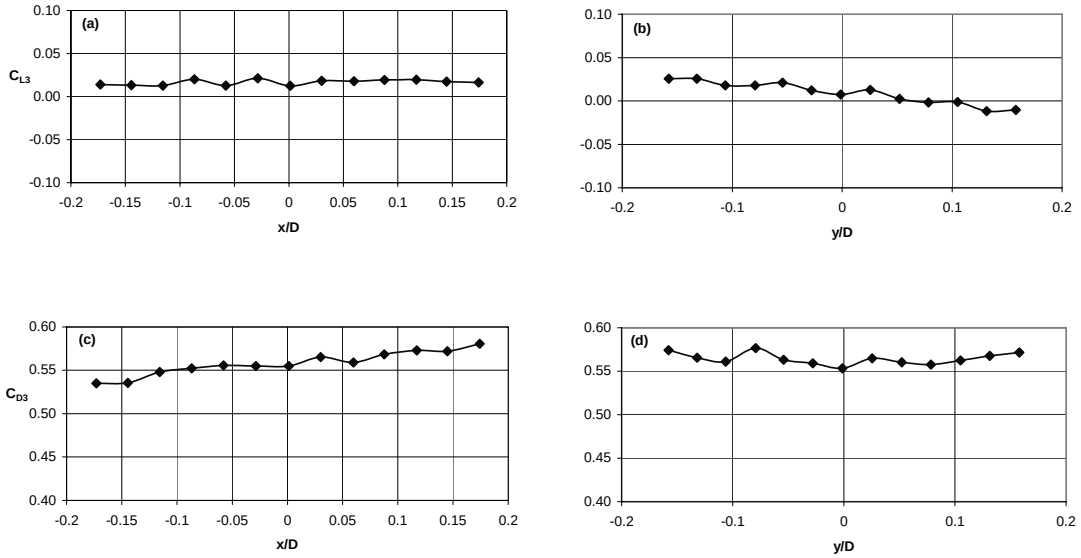

Fig. 11: The effect of tube 'C' displacement on the measured (a,b) lift and (c,d) drag force coefficients for tube 3 ($U_p = 3.96 m/s$, $\beta = 80\%$).

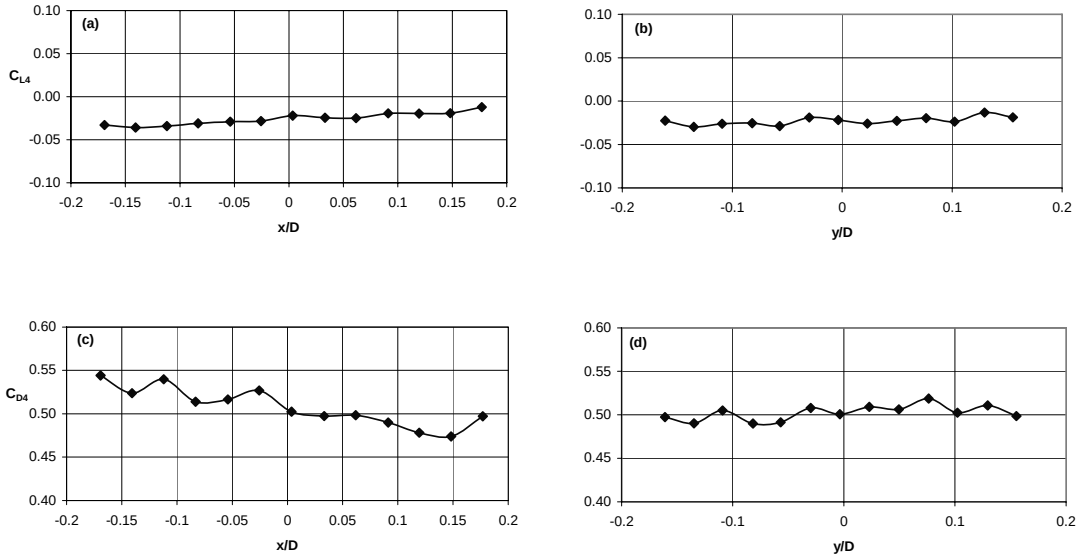

Fig. 12: The effect of tube 'C' displacement on the measured (a,b) lift and (c,d) drag force coefficients for tube 4 ($U_p = 3.96 m/s$, $\beta = 80\%$).

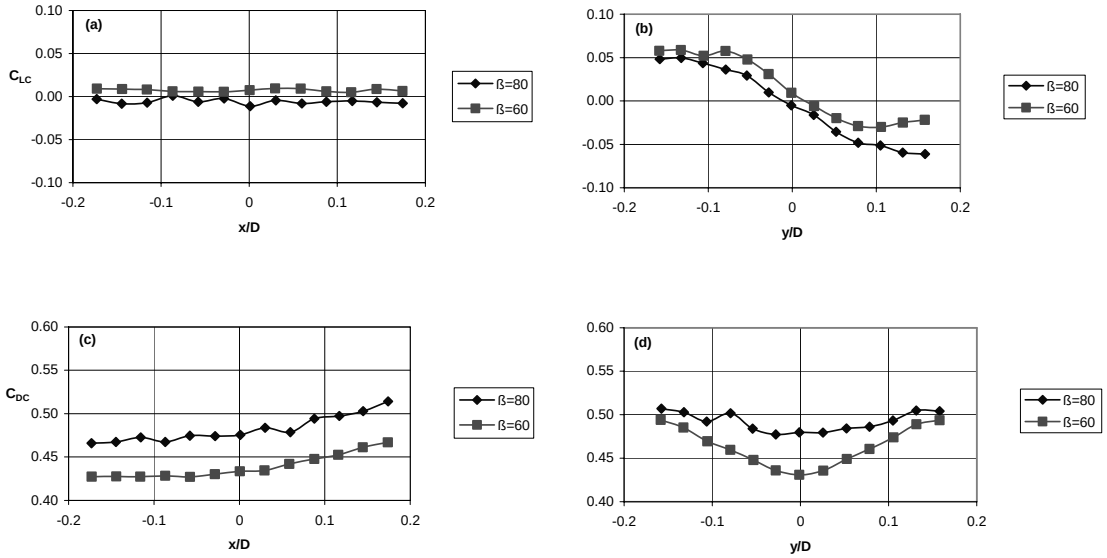

Fig. 13: Measured (a,b) lift and (c,d) drag force coefficients for central cylinder, 'C', comparison of ($U_P = 3.96m/s$, $\beta = 80\%$) and ($U_P = 3.92m/s$, $\beta = 60\%$).

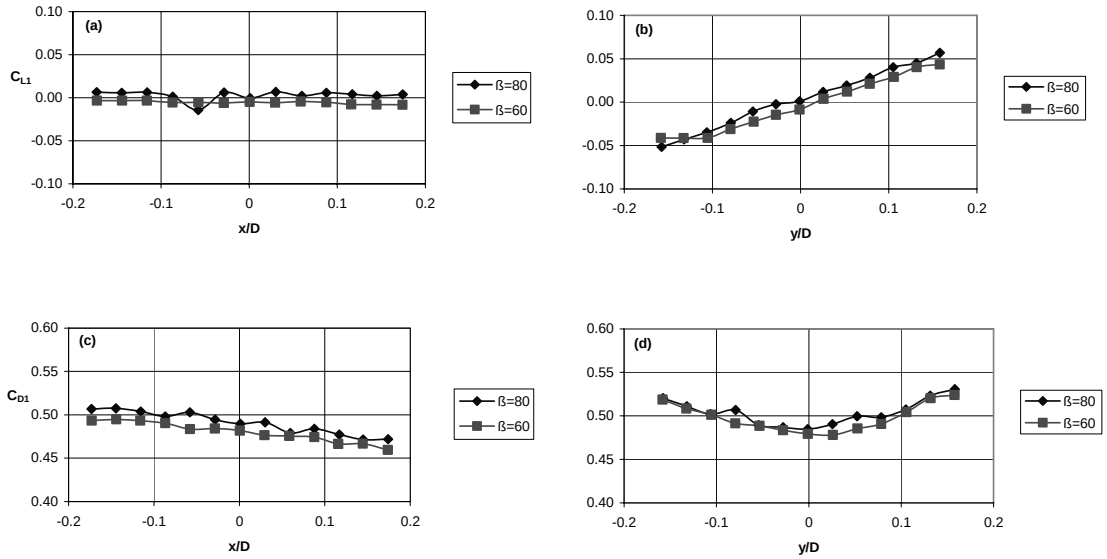

Fig. 14: The effect of tube 'C' displacement on the measured (a,b) lift and (c,d) drag force coefficients for tube 1 for ($U_P = 3.96m/s$, $\beta = 80\%$) and ($U_P = 3.92m/s$, $\beta = 60\%$).

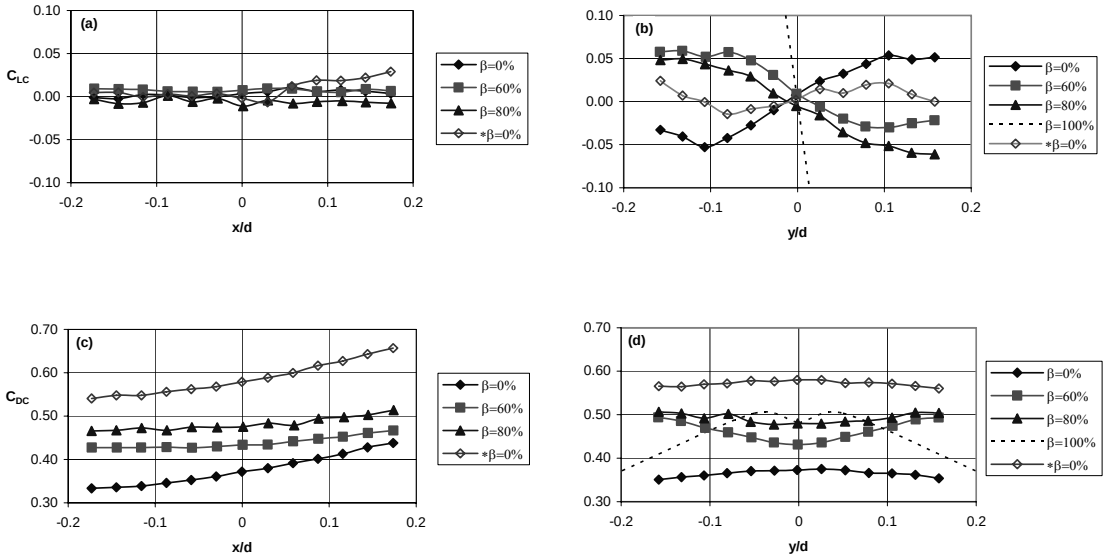

Fig. 15: Measured (a,b) lift and (c,d) drag force coefficients for central cylinder for ($U_P = 3.96m/s$, $\beta = 80\%$), ($U_P = 3.92m/s$, $\beta = 60\%$), ($U_P = 1.84m/s$, $\beta = 0\%$) and ($U_P = 1.84m/s$, $\beta = 0\%$); '*' indicates test without upstream mixer.

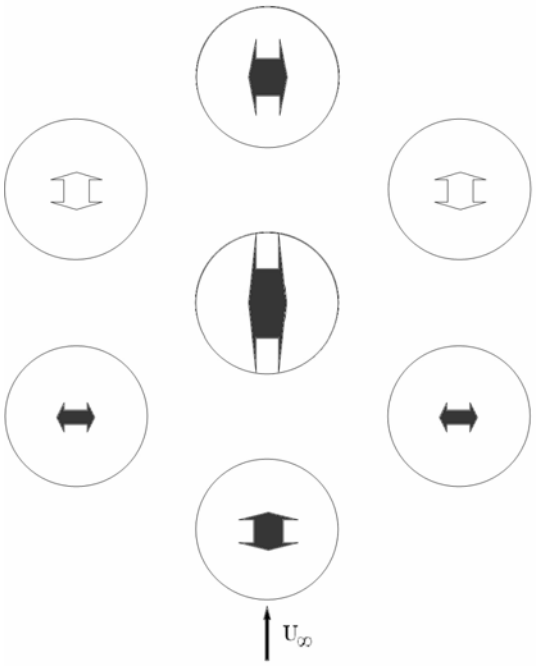

Fig. 16: Influence of tube 'C' on its neighbors for $\beta = 80\%$ each arrow indicates the magnitude and direction of the most important force derivative. Open arrows indicate that the cylinder 'C' direction of motion is normal to the cylinder force direction.

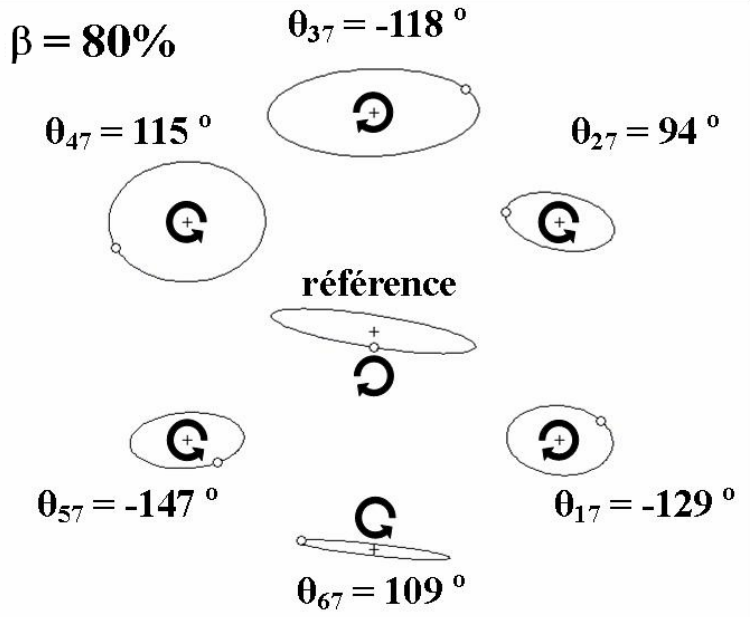

Fig. 17: Orbital motion of flexible tubes at instability for $\beta = 80\%$ **,** $U_{pc} = 7m/s$